Offshore Code Comparison Collaboration Continuation Within IEA Wind Task 30: Phase II Results Regarding a Floating Semisubmersible Wind System

Preprint

A. Robertson, J. Jonkman, F. Vorpahl, W. Popko, J. Qvist, L. Frøyd, X. Chen, J. Azcona, E. Uzunoglu, C. Guedes Soares, C. Luan, H. Yutong, F. Pengcheng, A. Yde, T. Larsen, J. Nichols, R. Buils, L. Lei, T. Anders Nygard, D. Manolas, A. Heege, S. Ringdalen Vatne, H. Ormberg, T. Duarte, C. Godreau, H. Fabricius Hansen, A. Wedel Nielsen, H. Riber, C. Le Cunff, R. Abele, F. Beyer, A. Yamaguchi, K. Jin Jung, H. Shin, W. Shi, H. Park, M. Alves, and M. Guérinel

To be presented at the 33rd International Conference on Ocean, Offshore and Arctic Engineering
San Francisco, California
June 8–13, 2014

NREL is a national laboratory of the U.S. Department of Energy, Office of Energy Efficiency & Renewable Energy, operated by the Alliance for Sustainable Energy, LLC.

Conference Paper
NREL/CP-5000-61154
March 2014

Contract No. DE-AC36-08GO28308

Available electronically at http://www.osti.gov/bridge

Available for a processing fee to U.S. Department of Energy
and its contractors, in paper, from:

U.S. Department of Energy
Office of Scientific and Technical Information
P.O. Box 62
Oak Ridge, TN 37831-0062
phone: 865.576.8401
fax: 865.576.5728
email: mailto:reports@adonis.osti.gov

Available for sale to the public, in paper, from:

U.S. Department of Commerce
National Technical Information Service
5285 Port Royal Road
Springfield, VA 22161
phone: 800.553.6847
fax: 703.605.6900
email: orders@ntis.fedworld.gov
online ordering: http://www.ntis.gov/help/ordermethods.aspx

Cover Photos: (left to right) PIX 16416, PIX 17423, PIX 16560, PIX 17613, PIX 17436, PIX 17721

Printed on paper containing at least 50% wastepaper, including 10% post consumer waste.

OFFSHORE CODE COMPARISON COLLABORATION CONTINUATION WITHIN IEA WIND TASK 30: PHASE II RESULTS REGARDING A FLOATING SEMISUBMERSIBLE WIND SYSTEM

Amy Robertson and Jason Jonkman
National Renewable Energy Laboratory
Golden, Colorado, USA

Fabian Vorpahl and Wojciech Popko
Fraunhofer Institute for Wind Energy and
Energy Systems Technology IWES
Bremerhaven, Germany

Jacob Qvist and Lars Frøyd
4subsea
Hvalstad, Norway

Xiaohong Chen
American Bureau of Shipping
Houston, Texas, USA

José Azcona
National Renewable Energy Centre
Navarra, Spain

Emre Uzunoglu and Carlos Guedes Soares
CENTEC, Instituto Superior Técnico
Universidade de Lisboa, Portugal

Chenyu Luan
CeSOS and NOWITECH
Trondheim, Norway

Huang Yutong and Fu Pengcheng
China General Certification Center
Beijing, China

Anders Yde and Torben Larsen
Technical University of Denmark
Roskilde, Denmark

James Nichols and Ricard Buils
DNV GL
Høvik, Norway

Liu Lei
Goldwind
Beijing, China

Tor Anders Nygaard
Institute for Energy Technology
Kjeller, Norway

Dimitris Manolas
National Technical University of Athens
Athens, Greece

Andreas Heege
SAMTECH s.a.
Barcelona, Spain

Sigrid Ringdalen Vatne and Harald Ormberg
MARINTEK
Trondheim, Norway

Tiago Duarte and Cyril Godreau
Instituto Superior Técnico,
Universidade de Lisboa
Lisbon, Portugal

Hans Fabricius Hansen and Anders Wedel Nielsen
DHI
Hørsholm, Denmark

Hans Riber and Cédric Le Cunff
PRINCIPIA NORTH
Svendborg, Denmark

Raimund Abele and Friedemann Beyer
University of Stuttgart
Stuttgart, Germany

Atsushi Yamaguchi
University of Tokyo
Tokyo, Japan

Kwang Jin Jung and Hyunkyoung Shin
University of Ulsan
Ulsan, Korea

Wei Shi and Hyunchul Park
POSTECH
Pohang, Korea

Marco Alves and Matthieu Guérinel
WavEC – Offshore Renewables
Lisbon, Portugal

ABSTRACT

Offshore wind turbines are designed and analyzed using comprehensive simulation tools (or codes) that account for the coupled dynamics of the wind inflow, aerodynamics, elasticity, and controls of the turbine, along with the incident waves, sea current, hydrodynamics, mooring dynamics, and foundation dynamics of the support structure. This paper describes the latest findings of the code-to-code verification activities of the Offshore Code Comparison Collaboration Continuation project, which operates under the International Energy Agency Wind Task 30. In the latest phase of the project, participants used an assortment of simulation codes to model the coupled dynamic response of a 5-MW wind turbine installed on a floating semisubmersible in 200 m of water. Code predictions were compared from load case simulations selected to test different model features. The comparisons have resulted in a greater understanding of offshore floating wind turbine dynamics and modeling techniques, and better knowledge of the validity of

various approximations. The lessons learned from this exercise have improved the participants' codes, thus improving the standard of offshore wind turbine modeling.

INTRODUCTION

The vast offshore wind resource represents a potential to use wind turbines installed offshore to power much of the world. Design standardization is difficult, however, because offshore sites vary significantly in regards to water depth, soil type, and wind and wave severity. To ensure that the cost of offshore wind turbine (OWT) installations is minimized, the use of a variety of support-structure types is required. These types include fixed-bottom monopiles, gravity bases, space-frames—such as tripods and lattice frames (e.g., "jackets")—and floating structures. In this context, the offshore wind industry faces many new design challenges.

Wind turbines are designed and analyzed using simulation tools (i.e., computer design codes) capable of predicting the coupled dynamic loads and responses of the system. The simulation tools that were developed to model land-based wind systems rely on the use of aero-servo-elastic codes, which incorporate wind-inflow, aerodynamic (aero), control system (servo), and structural-dynamic (elastic) models in the time domain in a coupled simulation environment. To accommodate the additional dynamics pertinent to offshore installations, these codes have been expanded to include the modeling of incident waves, sea current, hydrodynamics, and foundation dynamics of the support structure (see Figure 1). The high complexity and sophistication of these simulation codes underscores the need to verify and validate their accuracy. Two research tasks were developed under the International Energy Agency (IEA) Wind tasks to address this need: the Offshore Code Comparison Collaboration (OC3) and the Offshore Code Comparison Collaboration, Continuation (OC4) projects.

The OC3 project, which operated under the IEA Wind Task 23, Subtask 2, was the first international project to address the need to verify OWT modeling tools. The OC4 project was an extension of the original project and operated under IEA Wind Task 30. The purpose of the OC3 and OC4 projects was to verify the accuracy of OWT dynamics simulation codes through code-to-code comparison of simulated responses of various offshore structures. In this paper, the results from Phase II of the OC4 project, which involved the analysis of a 5-MW turbine supported by a floating semisubmersible, are presented. Twenty-one different organizations from 11 different countries submitted results using 19 different simulation codes. The variety of organizations contributing to the project brought together expertise from both the offshore structure and wind energy communities.

PARTICIPANTS AND CODES

The OC4 project was performed through technical exchange among a group of international participants from universities, research institutions, and industry across the United States, Germany, Denmark, the United Kingdom, Spain, the Netherlands, Norway, Sweden, Korea, Japan, Portugal, Greece, and China. The participants that contributed results for Phase II included: the National Renewable Energy Laboratory (NREL), the Centre for Marine Technology and Engineering (CENTEC), Instituto Superior Tecnico (IST), Goldwind, the

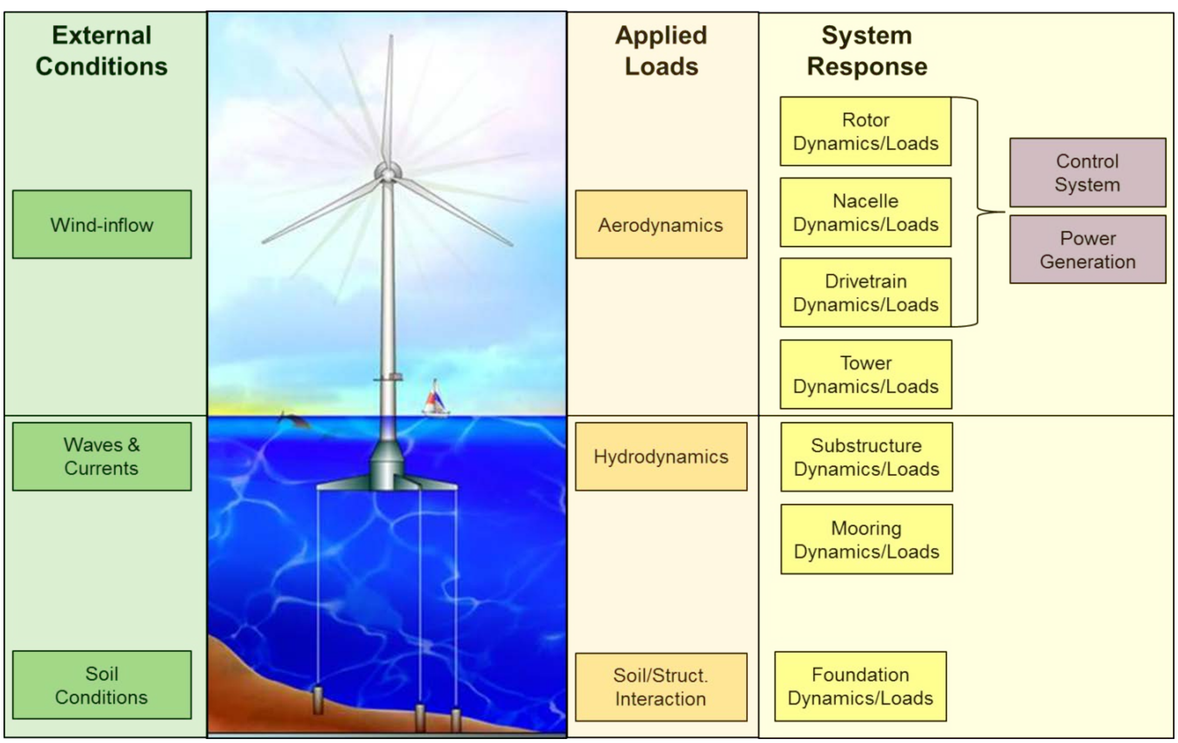

Figure 1: Diagram of the components of offshore wind modeling tools

American Bureau of Shipping (ABS), the National Renewable Energy Centre (CENER), the University of Ulsan (UOU), Garrad Hassan (GH), the China General Certification Center (CGC), Pohang University of Science and Technology (POSTECH), 4Subsea, the Technical University of Denmark (DTU), the National Technical University of Athens (NTUA), the Centre for Ships and Ocean Structures (CeSOS), Norwegian Marine Technology Research Institute (MARINTEK), the Institute for Energy Technology (IFE), SAMTECH s.a. with the Catalonia Institute for Energy Research (IREC), PRINCIPIA with IFP Energies nouvelles (IFPEN), the University of Stuttgart's Endowed Chair of Wind Energy at the Institute of Aircraft Design (SWE), the University of Tokyo, WavEC Offshore Renewables, Chonqing Haizhung Windpower Equipment co., LTD (CSIC), and DHI.

Most of the aero-hydro-servo-elastic codes that have been developed for modeling the dynamic response of offshore wind turbines were tested within OC4. Table 1 summarizes the existing modeling capabilities of the simulation tools used by (and in some cases, developed by) each participant for Phase II. In the cases where Table 1 shows the same code being used by multiple OC4 participants, the model development, simulation runs, and data processing were done independently.

Table 1: Overview of offshore wind modeling tool capabilities

Code	Code Developer	OC4 Participant	Structural Dynamics	Aerodynamics	Hydrodynamics	Mooring Model
FAST	NREL	NREL, CENTEC, IST, Goldwind, CSIC	T: Mod/MB P: Rigid	(BEM or GDW)+DS	PF + QD + (QTF)	QS
FAST v8	NREL	NREL	T: Mod/MB P: Rigid	(BEM or GDW)+DS	PF + ME	QS
CHARM3D+ FAST	TAMU+ NREL	ABS	T: Mod/MB P: Rigid	(BEM or GDW)+DS	PF + ME + (MD + NA) + (IP + IWL)	FE/Dyn
OPASS+ FAST	CENER+ NREL	CENER	T: Mod/MB P: Rigid	(BEM or GDW)+DS	PF + ME	LM/Dyn
UOU+FAST	UOU+NREL	University of Ulsan	T: Mod/MB P: Rigid	(BEM or GDW)+DS	PF + QD	QS
Bladed	GH	GH, CGC, POSTECH	T: Mod/MB P: MB	(BEM or GDW)+DS	ME + (IWL+ IP)	QS
Bladed Advanced Hydro Beta	GH	GH	T: Mod/MB P: MB	(BEM or GDW)+DS	PF + ME + (IWL)	QS
OrcaFlex	Orcina	4Subsea	T: FE P: Rigid	BEM, GDW, or FDT	PF + ME	LM/Dyn
HAWC2	DTU	DTU	T: MB/FE P: MB/FE	(BEM or GDW)+DS	ME	FE/Dyn
hydro-GAST	NTUA	NTUA	T: MB/FE P: MB/FE	BEM or FWV	PF + ME + (IP)	FE/Dyn
Simo+Riflex+ AeroDyn	MARINTEK+ NREL	CeSOS	T: FE P: FE	(BEM or GDW)+DS	PF+ME	FE/Dyn
Riflex-Coupled	MARINTEK	MARINTEK	T: FE P: Rigid	BEM+FDT	PF + ME + (IWL)	FE/Dyn
3Dfloat	IFE-UMB	IFE	T: FE (co-rotated) P: FE	BEM+FDT	ME + (IWL)	FE/Dyn
SWT	SAMTECH	SAMTECH & IREC	T: FE+Mod/MB P:FE+Mod/MB	BEM or GDW	ME + (IWL)	FE/Dyn
DeepLinesWT	PRINCIPIA-IFPEN	PRINCIPIA	T: FE P: FE	BEM+DS	PF + ME + (MD + QTF/NA) + (IP + IWL)	FE/Dyn
SIMPACK+ HydroDyn	SIMPACK	SWE	T: Mod/MB P: Rigid	BEM or GDW	PF + QD	QS
CAsT	University of Tokyo	University of Tokyo	T: FE W: FE	BEM	ME	QS
Wavec2Wire	WavEC	WavEC	T: N/A P: Rigid	N/A	PF + QD	QS
WAMSIM	DHI	DHI	T: N/A P: Rigid	N/A	PF + QD	QS

T = turbine P = platform Mod = modal MB = multi-body FE = finite element N/A = not applicable	BEM = blade-element/momentum GDW = generalized dynamic wake DS = dynamic stall FDT = filtered dynamic thrust FWV = free-wake vortex	PF = potential flow theory ME = Morison eq. MD = mean drift QTF = quadratic transfer function NA = Newman's approximation IP = instantaneous position IWL = instantaneous water level QD = quadratic drag	QS = quasi-static Dyn = dynamic LM = lumped mass

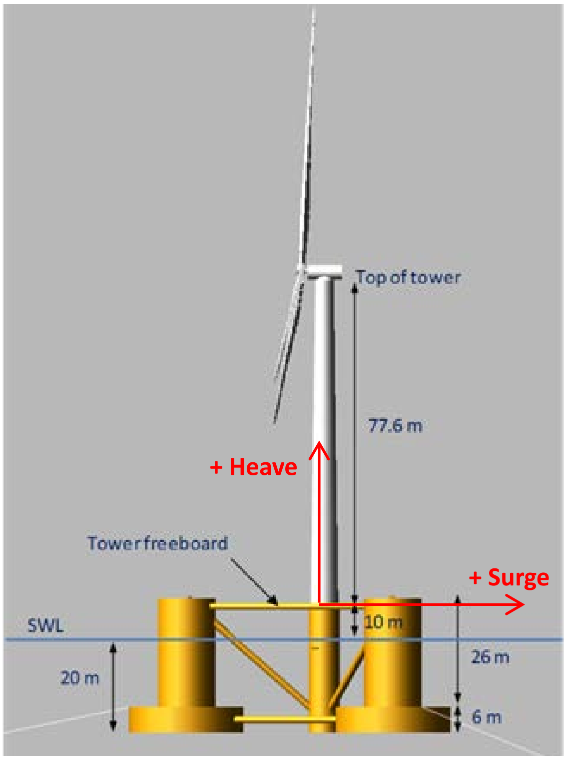

Figure 2: OC4-DeepCwind floating wind system design

Table 2: Summary of semisubmersible properties

Depth of platform base below SWL (total draft)	20 m
Elevation of main column (tower base) above SWL	10 m
Elevation of offset columns above SWL	12 m
Length of upper columns	26 m
Length of base columns	6 m
Depth to top of base columns below SWL	14 m
Diameter of main column	6.5 m
Diameter of offset (upper) columns	12 m
Diameter of base columns	24 m
Diameter of pontoons and cross braces	1.6 m
Platform mass, including ballast	1.3473E+7 kg
Platform CM location below SWL	13.46 m
Platform roll inertia about CM	6.827E+9 kg-m^2
Platform pitch inertia about CM	6.827E+9 kg-m^2
Platform yaw inertia about CM	1.226E+10 kg-m^2
Number of mooring lines	3
Angle between adjacent lines	120^0
Depth to anchors below SWL (water depth)	200 m
Depth to fairleads below SWL	14 m
Radius to anchors from platform centerline	837.6 m
Radius to fairleads from platform centerline	40.868 m
Unstretched mooring line length	835.5 m
Mooring line diameter	0.0766 m
Equivalent mooring line mass density	113.35 kg/m
Equivalent mooring line mass in water	108.63 kg/m
Equivalent mooring line extensional stiffness	7.536E+8 N

CODE-TO-CODE VERIFICATION PROCESS

The simulation of offshore wind turbines under combined aerodynamic and hydrodynamic loading is complex. The OC4 task, therefore, requires a sophisticated approach that facilitates the identification of sources of modeling discrepancies introduced by differing theories and model implementations in the various codes. This is possible only by meticulously controlling all of the inputs to the codes and by carefully applying a stepwise verification procedure where model complexity is increased in each step.

The code-to-code verification process is performed as follows. First, an offshore wind system design of interest is identified, and the information needed to model the system is developed and shared with the project partners. Second, a set of simulations (load cases) is defined to test the response behavior of the system. The simulations encompass system-identification tests and a stepped approach for examining the system response to wind excitation, wave excitation, and the combination of the two. In addition, to examine the influence of system elasticity and its interaction with the offshore environment, different components of the system are modeled as flexible or rigid within the load cases. Various environmental conditions are used to examine the response behavior in both benign and extreme conditions. Next, the participants build a model of the given design in their respective modeling tools and run the prescribed load cases. The simulated response behavior (loads/motions) is then compared among the various codes at multiple points throughout the system. This allows mistakes in the modeling implementation or simulation settings to be identified, shows differences in the resulting loads/motions based on the modeling approach, and spurs discussion about the differences between and applicability of the various modeling theories. This procedure was repeated for multiple offshore wind system designs within the OC3 and OC4 projects. Through this process, an understanding of the applicability of modeling theories was developed, changes were made to the tools, and future tool improvement needs were identified.

OC4 PHASE II OVERVIEW

Semisubmersible Description

Phase II of the OC4 project involved the modeling of a semisubmersible floating offshore wind system developed for the DeepCwind project [1] as shown in Figure 2. This concept was chosen for its increased hydrodynamic complexity compared to the only other floating system analyzed in the OC3 and OC4 projects, the OC3-Hywind spar buoy [2]. A summary of the semisubmersible's properties can be found in Table 2 and in the description document that was disseminated to the group [3]. (Note that SWL represents the still water level and CM represents the center of mass of the semisubmersible platform only.)

DeepCwind is a U.S.-based project aimed at generating experimental and field-test data for use in validating floating OWT modeling tools. The semisubersible and two other floating designs were tested by the DeepCwind project in a series of scaled tank tests at MARIN in 2011 [1]. The wind turbine modeled in OC4 is the NREL 5-MW offshore baseline turbine [4], which differs slightly from the scaled one tested by DeepCwind. This turbine was used in all phases of the OC3 and OC4 projects, but the control system logic and tower properties changed to accommodate the differences in system dynamics.

Load Case Descriptions

To compare the response behavior achieved by the different modeling approaches, 21 different load cases (simulations) were performed, encompassing varying levels of model complexity and a variety of metocean conditions. Table 3 summarizes these load cases. The cases are ordered in increasing complexity, with three distinct groupings. Group 1.X encompasses a set of simulations focused on system identification, including an eigenanalysis, a static equilibrium simulation, and a series of free-decay simulations. All simulations are run in the absence of air, with still water, and with the generator locked (a brake is applied). Group 2.X focuses on the interaction of the waves with the platform in the absence of wind. For these simulations, the platform, moorings, and tower are flexible, but the nacelle, drivetrain, and rotor are rigid and the generator is locked. The simulations include regular waves, irregular waves, and current. The last group, 3.X, examines the system with all relevant degrees of freedom (DOFs) enabled, and with combined wind and wave excitation. A variety of conditions are examined including both regular and irregular waves, steady and turbulent wind, current, and some damage scenarios. (Wind-only simulations with the

Table 3: Load cases run in OC4 Phase II

Load Case	Description	Enabled DOFs	Wind Condition	Wave Condition
1.1	Eigenanalysis	All	No air	Still water
1.2	Static equilibrium	All	No air	Still water
1.3a	Free decay, surge	Platform and moorings	No air	Still water
1.3b	Free decay, heave	Platform and moorings	No air	Still water
1.3c	Free decay, pitch	Platform and moorings	No air	Still water
1.3d	Free decay, yaw	Platform and moorings	No air	Still water
2.1	Regular waves	Support structure	No air	Regular airy: H = 6 m, T = 10 s
2.2	Irregular waves	Support structure	No air	Irregular airy: H_s = 6 m, T_p = 10 s, γ=2.87, JONSWAP spectrum
2.3	Current only	Support structure	No air	Surface = 0.5 m/s, 1/7th power law decrease with depth
2.4	Current and regular waves	Support structure	No air	Regular airy: H = 6 m, T = 10 s; current at surface = 0.5 m/s, 1/7th power law
2.5	50-year extreme wave	Support structure	No air	Irregular airy: H_s = 15.0 m, T_p = 19.2 s, γ=1.05, JONSWAP spectrum
2.6	RAO estimation, no wind	Support structure	No air	Banded white noise, PSD =1 m^2/Hz for 0.05-0.25 Hz
3.1	Deterministic, below rated	All	Steady, uniform, no shear: V_{hub} = 8 m/s	Regular airy: H = 6 m, T = 10 s
3.2	Stochastic, at rated	All	Turbulent (Mann model): V_{hub} = V_r (11.4 m/s)	Irregular airy: H_s = 6 m, T_p = 10 s, γ=2.87, JONSWAP spectrum
3.3	Stochastic, above rated	All	Turbulent (Mann model): V_{hub} = 18 m/s	Irregular airy: H_s = 6 m, T_p = 10 s, γ=2.87, JONSWAP spectrum
3.4	Wind/wave/current	All	Steady, uniform, no shear: V_{hub} = 8 m/s	Regular airy: H = 6 m, T = 10 s; current at surface = 0.5 m/s, 1/7th power law
3.5	50-year extreme wind/wave	All	Turbulent (Mann model): V_{hub} = 47.5 m/s	Irregular airy: H_s = 15.0 m, T_p = 19.2 s, γ=1.05, JONSWAP spectrum
3.6	Wind/wave misalignment	All	Steady, uniform, no shear: V_{hub} = 8 m/s	Regular airy: H = 6 m, T = 10 s, direction = 30^0
3.7	RAO estimation, with wind	All	Steady, uniform, no shear: V_{hub} = 8 m/s	Banded white noise, PSD =1 m^2/Hz for 0.05-0.25 Hz
3.8	Mooring line loss	All	Steady, uniform, no shear: V_{hub} = 18 m/s	Regular airy: H = 6 m, T = 10 s
3.9	Flooded column	All	Turbulent (Mann model): V_{hub} = 8 m/s	Irregular airy: H_s = 6 m, T_p = 10 s, γ=2.87, JONSWAP spectrum
RAO = response amplitude operator			V_{hub} = hub-height wind speed V_r = rated wind speed PSD = power-spectral density	H = wave height H_s = significant wave height T = wave period T_p = peak-spectral wave period γ = peak enhancement factor

NREL 5-MW turbine were compared within the OC3 project and were not repeated in OC4 Phase II.)

In all load cases, the turbine is initially facing perfectly upwind (no yaw error), and in all but one load case, the direction of the waves is aligned with the wind. The only exception to this is load case 3.6, in which the waves are offset from the wind by 30 deg. Turbulent wind and irregular wave time histories were provided to the group, but some participants generated their own files based on the parameters provided.

Hydrodynamic Modeling Approaches

One of the main outcomes of OC4 Phase II is a better understanding of the influence of hydrodynamic modeling approaches on the response of a floating semisubmersible. These findings are reviewed in the next section, but first an overview of the modeling theories employed by the participants is given here.

The hydrodynamic loads on a floating structure include excitation from incident waves, radiation of outgoing waves from platform motion (including added mass and damping effects), and viscous forces. Two general techniques are commonly used for modeling these loads, potential-flow theory and Morison's equation. The applicability of these two theories is dependent on the size of the structure being modeled and the water flow regime. The simulation tools used in this project employ one of these two methods, or a combination of the two.

When the size of the structure in the water is large compared to the wavelength, the water will remain attached as it flows past the structure, and potential-flow theory is applicable. Panel methods are the most common technique for modeling potential loads. Often, only the linear portion of the potential-flow solution is used in offshore wind simulations. Some codes, however, offer the option of including second-order terms, or an approximation of the difference-frequency terms through Newman's approximation. The second-order approach results in mean forces being applied to the structure and excitation of the structure at sum/differences of pairs of wave frequencies. The mean-drift component can also be calculated directly from the linear solution. A potential-flow model will capture excitation from waves (including diffraction) and radiation (including added mass and damping effects), but does not capture the viscous drag on the structure resulting from flow separation. Therefore, codes using this approach alone have applied a global quadratic drag to the structure as an approximation.

For smaller structures, where flow separation occurs, Morison's equation is typically employed. Morison's equation is an empirically derived hydrodynamic loading model that includes excitation from waves (with a long wavelength approximation), added mass effects, and viscous forces. The theory can be enhanced by integrating the Morison forces up to the instantaneous water surface elevation using a wave stretching approach and/or by applying the forces at the instantaneous position of the displaced body in the water. The inclusion of these methods results in higher order loads (including a mean-drift force) on the structure. When using this method alone, one must be sure to also account for both the hydrostatic forces and dynamic pressure loads.

The applicability of these two modeling approaches can be assessed through three dimensionless parameters, the Keulegan-Carpenter number, the Reynolds number, and the diameter-to-wavelength ratio. These parameters define the relative importance of inertia, diffraction, and drag for different flow regimes. For the semisubmersible structure studied here, it was found that either of these approaches (or a combination) can be used to accurately model the hydrodynamic loads on the structure. For codes using a combined-theory approach, the potential-flow solution is used to model the radiation and diffraction loads, while Morison's equation is used to model the viscous-drag loads.

RESULTS

Each of the participants ran the prescribed load cases using the models they had built in their modeling tool of choice. The simulated response behavior (loads/motions) was then compared between the various codes at multiple points throughout the system. A subset of these results is summarized in the plots in this section (full results are available in [5]). In these plots, a unique color is assigned to the result from a given participant, as shown in the legend in Figure 3. In the bar plots, the results are presented as a solid color, but in the line plots, the results use either a solid, dotted, or dash-dot line, based on the type of hydrodynamic model being used in the tool. A solid line represents a code that uses a potential-flow theory approach, dotted is for Morison-only, and dash-dot is for codes that use a combination of the two. Some tools have the option of using different theories, so some participants have supplied two different results from the same code with differing hydrodynamic models.

For the free-decay and deterministic wind/wave simulations, time series were compared. For the stochastic wind/wave simulations, the results were compared using PSDs of the responses (with the application of some smoothing functions). In addition, this project included the computation of response amplitude operators (RAOs) both in wave-only and combined wind/wave conditions.

The delineation of the responses in the plots based on the hydrodynamic model used suggests the importance of the model on the results seen in the simulations. The large motion of floating structures and the complexity of this floating design create a complex hydrodynamics problem. In the simulations it was found that the differences in the hydrodynamic theories were more significant among the modeling tools than the aerodynamic or structural theories. Therefore, the results presented in this section largely focus on the system response due to wave loads. Some wind cases are covered, especially in terms of how adding wind affects the response of the system when compared to a wave-only simulation.

Full-System Eigenanalysis (Load Case 1.1)

Figure 3 shows a selection of the lowest natural frequencies of the OC4-DeepCwind semisubmersible in still water and no wind (load case 1.1). The rigid-body frequencies of the system (upper plot of Figure 3) are fairly consistent, with the exception of the roll and pitch motions for POSTECH and the University of Tokyo. The University of Tokyo investigators have identified an issue with modeling the pitch moment of inertia in their code, which also affects the blade's natural frequencies.

Larger differences are seen in the tower and turbine flexible frequencies, with some codes not capturing all of the flexible modes requested. Very few codes identify the tower torsion DOF, and there is little consistency between the results provided. PRINCIPIA and IFE's values show the coupling between the tower torsion and the blade asymmetric flapwise yaw mode. The largest variability in identified mode values is for the second bending modes of the tower. These modes are most likely more sensitive to the various methods being used to model the flexibility of the structure.

Free Decay (Load Case 1.3)

Four different free-decay simulations were run in load case 1.3, in which the system was offset by a prescribed amount, and then released to return to its equilibrium position. The simulations investigated included separate offsets for surge, heave, pitch, and yaw; however, each simulation has all platform and mooring DOFs enabled. These simulations are useful in demonstrating the rigid-body natural frequencies of the system, and their associated damping.

Figure 4 and Figure 5 show the surge, pitch, and heave motion results of the surge free-decay and heave free-decay simulations, respectively. The differences between the results are caused by two main factors, the hydrodynamic modeling approach used and the mooring line modeling approach used. These influences are most easily seen in the damping behavior of the results. The damping of the larger-motion response of the structure is more strongly influenced by the (quadratic) viscous

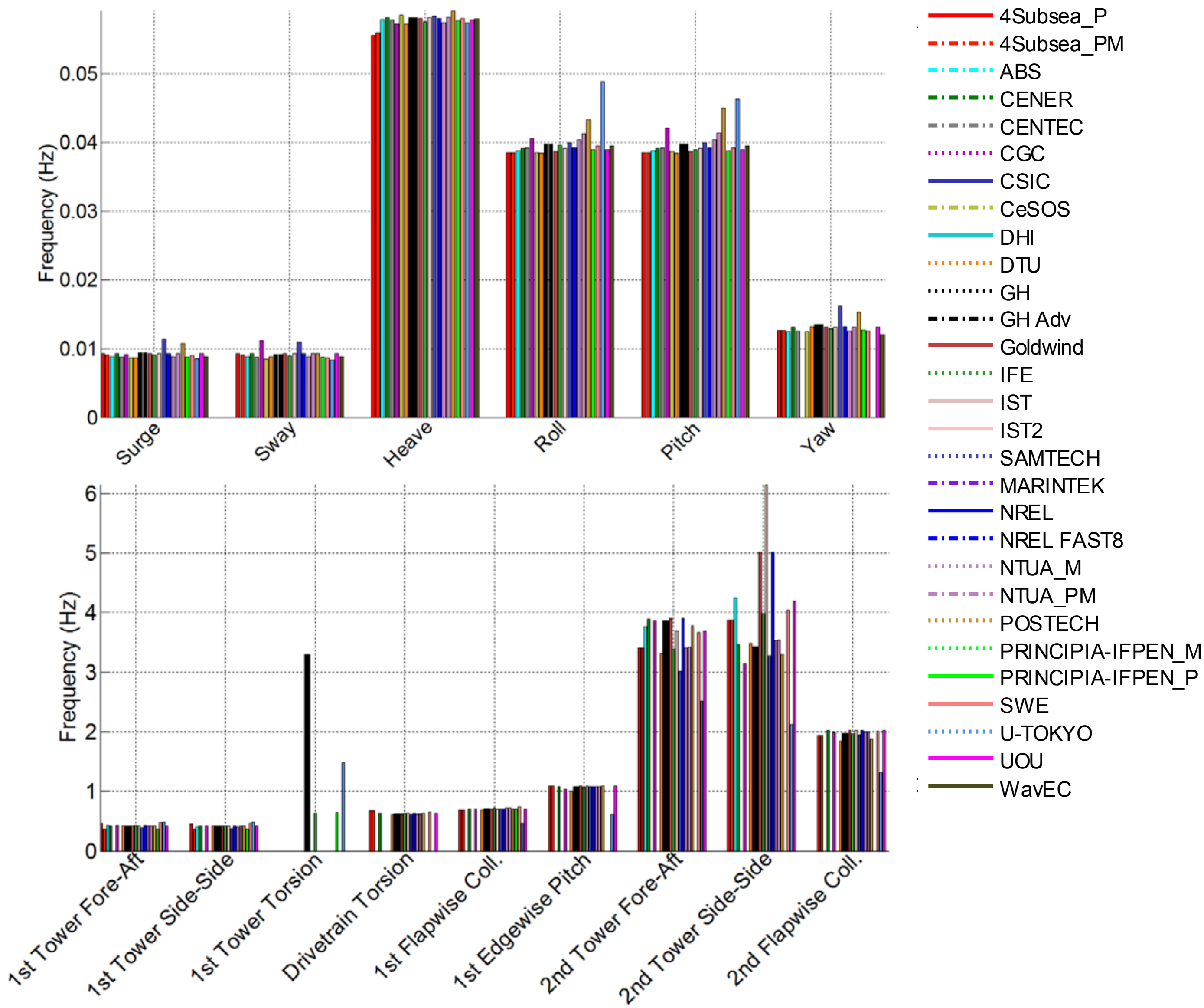

Figure 3: Full-system natural frequencies from load case 1.1

loads on the structure, whereas the smaller amplitude motion is more governed by (linear) radiation damping.

Generally, for the surge free-decay results, the results are very similar between the codes, with the exception of POSTECH and WavEC for the coupled responses in heave and pitch. There is no significant grouping of the responses because of the modeling approaches used.

For the heave free-decay simulations, the heave response itself is very similar, with the exception of PRINCIPIA, which employed a different radiation damping value. Larger differences are seen in the coupled responses to surge and pitch. For pitch, a very distinct grouping is seen for codes using Morison's equation for calculating the viscous drag (dotted or dash-dotted results) versus those using a quadratic drag matrix (solid line results). The different levels of damping most likely result from a lack of off-diagonal terms in the quadratic drag matrix. Potential-only solutions do not model the coupled pitch damping during heave motion.

In general, one can see that the differing modeling theories for hydrodynamics and mooring loads do not strongly influence the free-decay responses.

Regular Waves (Load Case 2.1)

Load case 2.1 examines the response of the semisubmersible when excited by regular (periodic) waves with

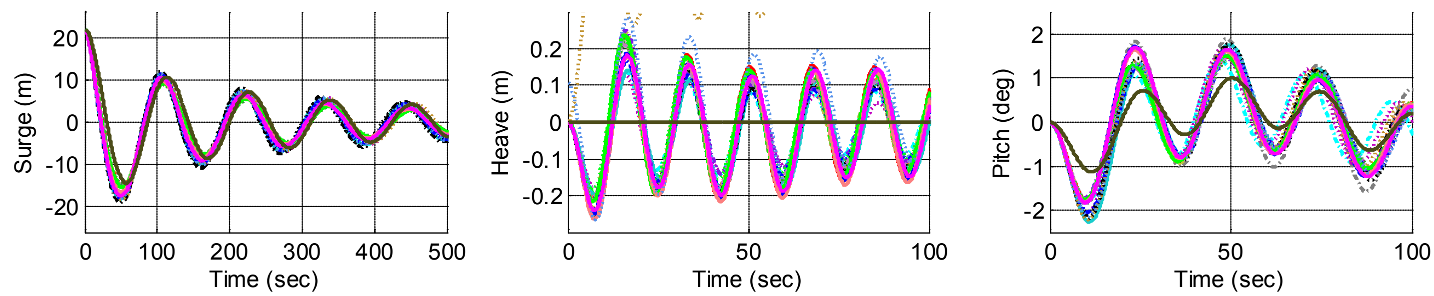

Figure 4: Surge free decay (load case 1.3a), platform motion response

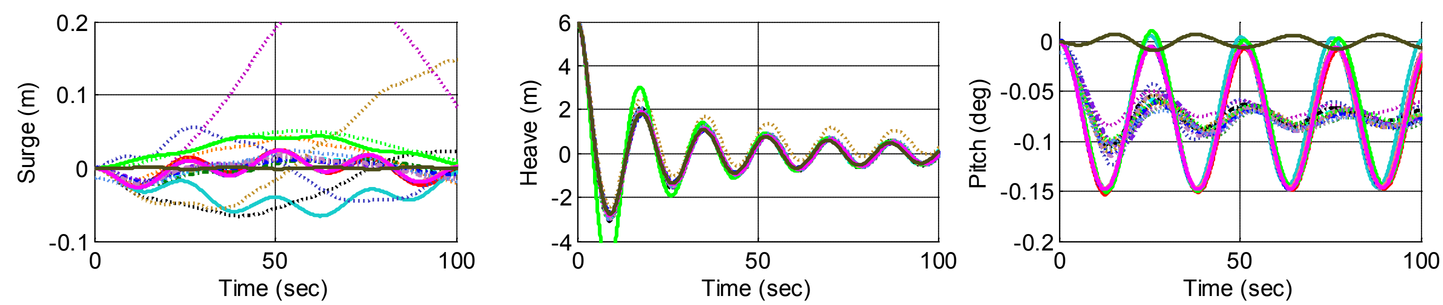

Figure 5: Heave free decay (load case 1.3b), platform motions response

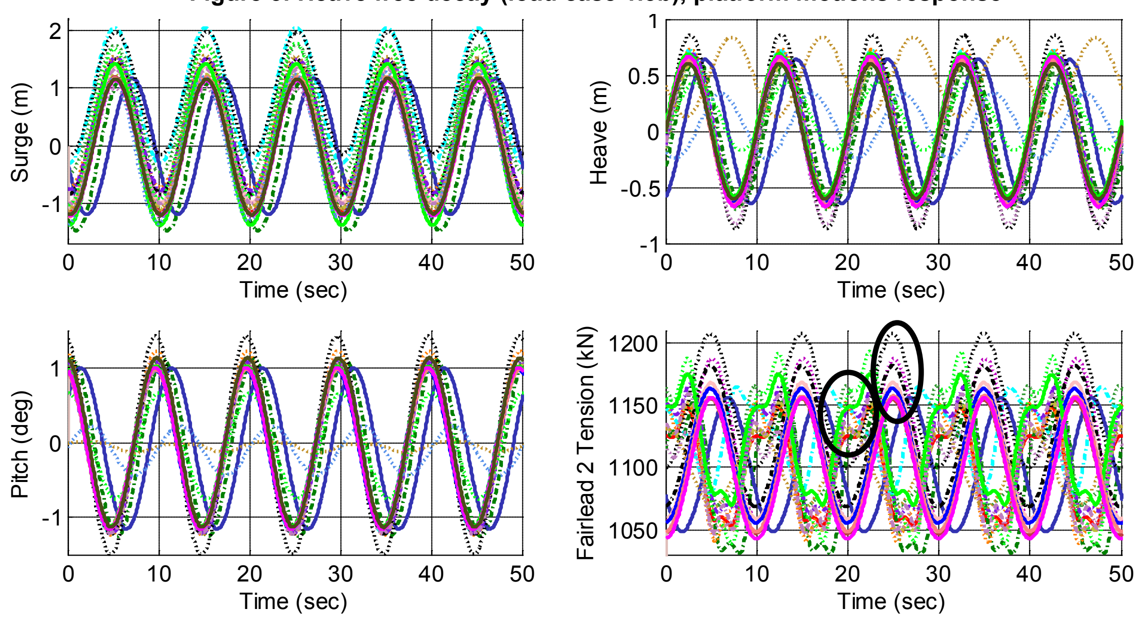

Figure 6: Regular wave simulation (load case 2.1), H = 6 m, T = 10 s

a height of 6 m and a period of 10 s. No wind was used in this simulation, and the turbine DOFs were turned off. Therefore, the modeling components of importance are once again the hydrodynamic and mooring models.

Figure 6 shows the surge, heave, and pitch responses of the semisubmersible for load case 2.1, as well as the tension of the second mooring line at the fairlead, which is the upwind mooring line oriented along zero-degree wind/waves. The surge response shows large differences between the different codes, based on whether drift forces are being accounted for in the hydrodynamic modeling approach. The surge response for simulations using first-order potential flow-theory and/or Morison's equation calculated at the undisplaced position of the body without wave stretching will oscillate about a zero-mean position. Realistically, however, the system will drift slightly, a nonlinear phenomenon that is captured through one of the following modeling approaches:

- Inclusion of second-order terms in the potential-flow theory solution
- Approximation of difference-frequency terms through Newman's approximation
- Application of a mean-drift force derived from first-order potential-flow theory
- Application of Morison's equation, both at the mean or instantaneous position of the body
- Integration of Morison's equation up to the instantaneous elevation of the wave using a stretching technique

Only codes that include one of these components have a non-zero mean value for the surge displacement. Two codes have much larger offsets than the others, ABS and GH. ABS includes every one of the methods described previously for accounting for drift forces, with the exception of the direct inclusion of second-order terms in the potential-flow solution. Most other codes include only the second-order difference terms in the potential-flow solution (IST2), Newman's approximation, or the application of ME at the instantaneous position and wave elevation.

The heave response to regular waves is more consistent, with only a couple of Morison-only codes, POSTECH and University of Tokyo, showing distinctly different results. This difference is assumed to be caused by incorrectly accounting for the variation in dynamic pressure on the base columns of the semi. This problem was encountered early in the project when many more of the Morison-only codes were under-predicting the heave response of the system in regular waves.

The fairlead tension for this load case demonstrates the differences between the mooring model used, whether a quasi-static solution is employed or one that considers the dynamics of the line as well as the excitation of the line from the waves. This differentiation is seen in the two distinct groupings of the response, as indicated by the circles in the figure. Those codes using a dynamic solution are out of phase with the quasi-static solutions, and include more frequencies in the response behavior beyond the wave frequency. Although the mooring loads may differ vastly between these two approaches, the mean values are similar and tend to have no significant effect on the overall dynamic response of the structure.

Stochastic Wind/Waves (Load Case 3.2)

To this point, the description of the results has focused on the global response of the structure, and has not covered the loads and motion of the turbine itself. This is because the turbine response is more similar between the codes than these global motions. But for completeness, this section shows a sample of wind turbine response behavior for a load case (3.2) in which the turbine is excited by irregular waves (H_s = 6 m, T_p = 10 s) and stochastic wind (V = 11.4 m/s).

Figure 7 shows the PSD of the out-of-plane deflection of blade 1. The results are fairly similar between the codes, but the different solutions deviate more as frequency increases. The higher responses come from those codes that use a quasi-steady BEM approach for their aerodynamic induction model, while the lower responses are those that use a form of dynamic wake theory. This is to be expected because the dynamic wake

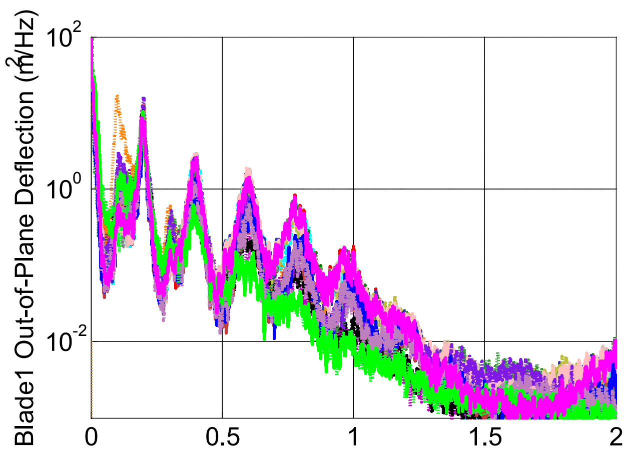

Figure 7: PSD of blade out-of-plane motion for stochastic wind/wave simulation (LC 3.2)

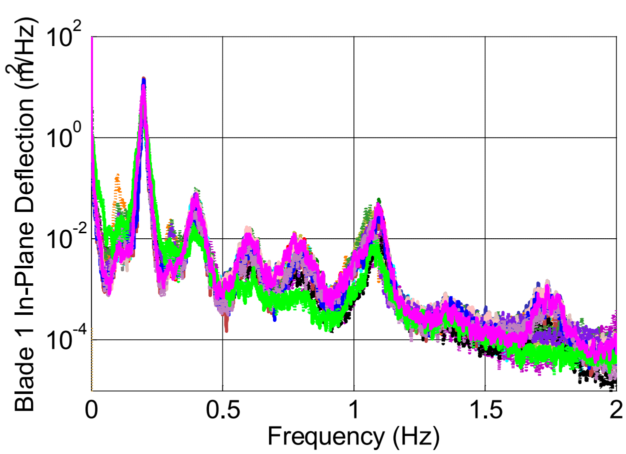

Figure 8: PSD of blade in-plane motion for stochastic wind/wave simulation (LC 3.2)

theory delays the response of the turbine to sudden changes in the wind, effectively damping the higher frequency response. Similar results are seen for the in-plane bending of the blade in Figure 8.

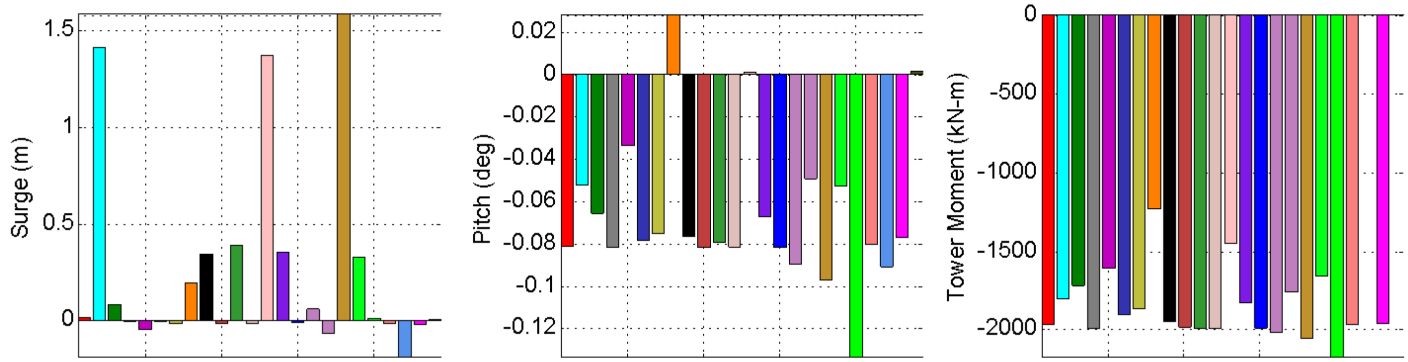

Figure 9: Irregular wave simulation (load case 2.2), H_s = 6 m and T_p = 10 s, mean value of response

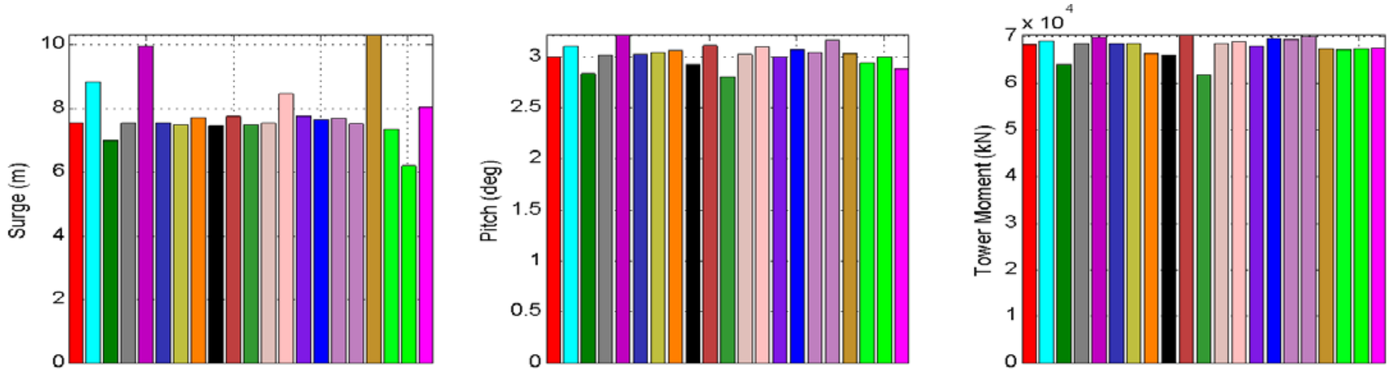

Figure 10: Irregular wave simulation with wind (load case 3.2), H_s = 6 m, T_p = 10 s, V=11.4 m/s, mean value of response

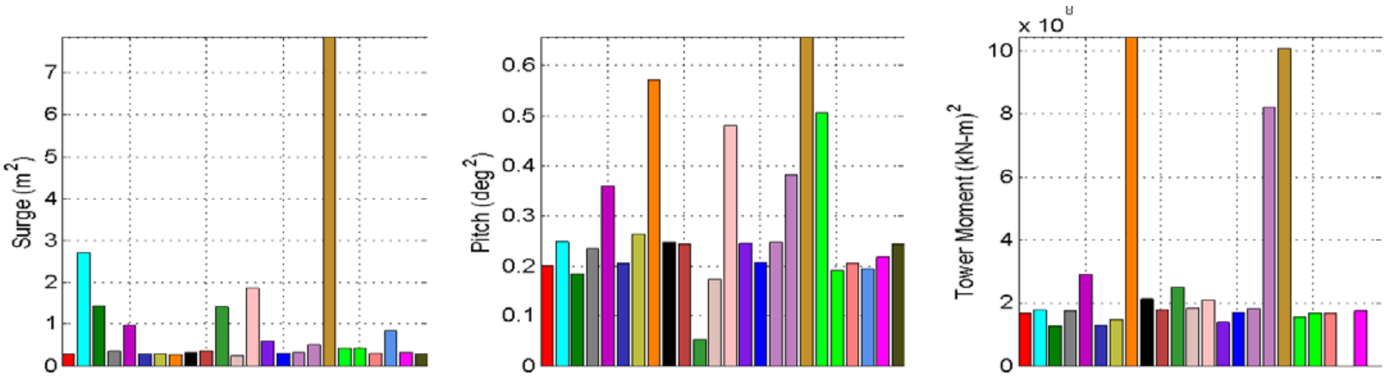

Figure 11: Irregular wave simulation (load case 2.2), H_s = 6 m and T_p = 10 s, variance of response

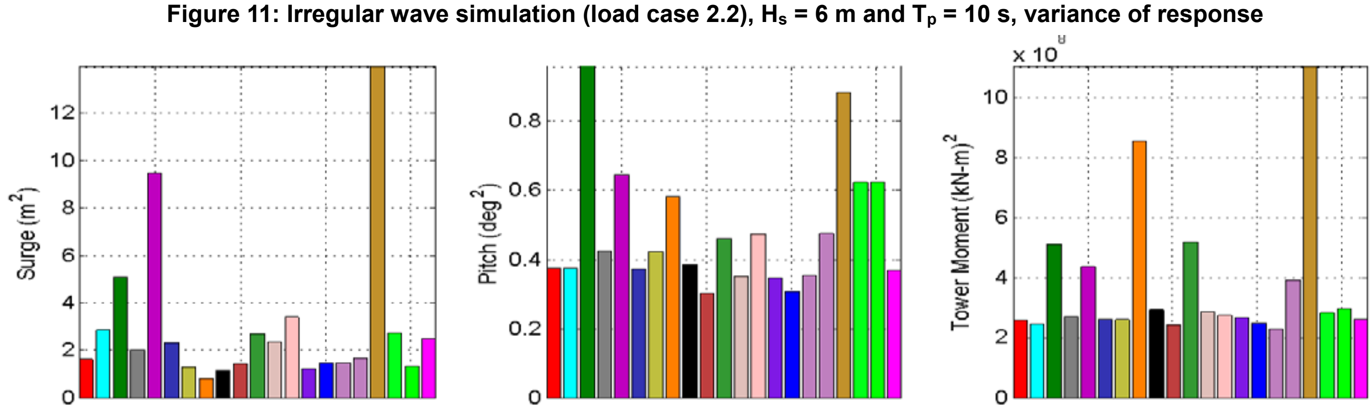

Figure 12: Irregular wave simulation with wind (load case 3.2), H_s = 6 m, T_p = 10 s, V=11.4 m/s, variance of response

Irregular Waves (Load Cases 2.2 and 3.2)

The next set of simulations examined involves irregular waves, both with and without wind. Figure 9 shows the mean value of select responses (surge, pitch, and tower bending in the fore/aft direction) to an irregular wave modeled using a JONSWAP spectrum with a significant wave height (H_s) of 6 m, and a peak-spectral period (T_p) of 10 s. Figure 10 then shows the same results, but with turbulent wind present for the operating turbine at rated wind speed (11.4 m/s).

In these figures, note that when wind is included, the offsets and loads increase significantly because of the thrust force of the wind on the turbine. The wind also equalizes the results among the participants, masking the differences seen when only waves are present (because the thrust force is much higher than the mean-drift force). The case without wind shows larger differences between the codes. The outliers from DTU probably result from an incorrectly prescribed axis definition for the output, and those in the surge response are largely caused by the drift effects discussed for the regular wave results.

Figure 11 and Figure 12 then show the variance (square of the standard deviation) of the system responses for these two simulations, which is an indicator of fatigue loading. A larger variance is seen in the response with wind present, especially for the surge motion, and there is more discrepancy among the different codes. These differences could be caused by variations in the underlying aerodynamic theories or by not eliminating all start-up transients in some results. The significant differences between the results for both the mean value and variance of the tower bending are concerning because this is a major component in the design of an offshore wind system.

Response Amplitude Operators (Load Cases 2.6 and 3.7)

RAOs are the ratio of system response to wave amplitude (resulting from wave excitation) and are commonly used during the design process in the offshore oil and gas industry to assess the linear wave-body response of floating platforms in the frequency domain. For this project, the RAOs were produced through the excitation of the system using a banded white-noise spectrum between 0.05 and 0.25 Hz (see wave height PSD in Figure 13). Further information on how the RAOs were calculated can be found in [6].

Figure 13 and Figure 14 show the computed RAOs for the semisubmersible both with and without wind (steady, 8 m/s) for a selection of output responses. Only the frequency band that was excited by the waves is shown in these plots. The information outside this band is meaningless since it would require a division by zero (or almost zero) to achieve.

In general, the wind excitation used here has very little effect on the RAOs, with the most significant change being seen in the mooring response for those using a dynamic model. There is a clear grouping in the mooring tension results for codes using dynamic versus quasi-static mooring models. The most significant difference is in the higher frequency region around 0.17 Hz, where the quasi-static results greatly underpredict the mooring loads in the system. This result suggests the need for a dynamic mooring model to accurately capture both the extreme and fatigue loads in the moorings. The surge and heave responses show some variation between the different codes, but the pitch and tower-bending moment are much more varied.

Significant variation is not expected in these RAOs because the focus has been only on the wave-excitation region where linear wave loads dominate the response. This is well covered by all modeling approaches. Examining the response of the semisubmersible outside the wave-excitation region reveals more differences in the response of the structure based on the modeling approach employed. In Figure 15 and Figure 16, the PSDs of the outputs examined in the RAO plots are shown for the frequency band from 0 to 0.5 Hz. The wave-excitation region (0.05 – 0.25 Hz) can be clearly seen in drop-offs in the response for the surge and mooring tension PSDs.

The surge and pitch natural frequencies are seen in their respective PSDs at 0.01 and 0.04 Hz, which are outside the wave-excitation region and are therefore excited by some form of nonlinear effect. One source is nonlinear hydrodynamic wave loads produced from Morison's equation or from higher-order terms in the potential-flow solution. In addition, it was found that codes using a Morison-only approach for calculating the hydrodynamic forces had an overall increased level of response in the pitch motion at frequencies outside the wave-excitation region, and to a lesser degree the surge motion.

The heave PSD, on the other hand, shows very little difference between the simulated responses because the heave natural frequency lies within the linear wave-excitation region at 0.058 Hz. The mooring tension PSD again clearly shows groupings in the higher frequencies based on whether a dynamic model is used (the two circles in Figure 15 show quasi-static and dynamic groupings), but the response in the low-frequency region is dominated by the surge/pitch behavior of the structure. The PSD of the tower-bending moment in the fore/aft direction, which is largely dictated by the pitching motion of the structure and therefore has similar behavior to that PSD, is also shown in the figure. More noticeable here, though, is the first bending natural frequency of the tower around 0.43 Hz. This frequency peak is also outside the wave-excitation region, and its magnitude is extremely varied between the different codes. Consistent with the pitch PSD, those codes using a Morison approach and/or some form of nonlinear hydrodynamic loading have an increased response. The solution from Marintek is an exception, showing no peak for the tower-bending moment natural frequency.

The PSD results outside the wave-excitation region are much more heavily affected by wind than the RAOs. This is especially true for the pitch response and the tower bending.

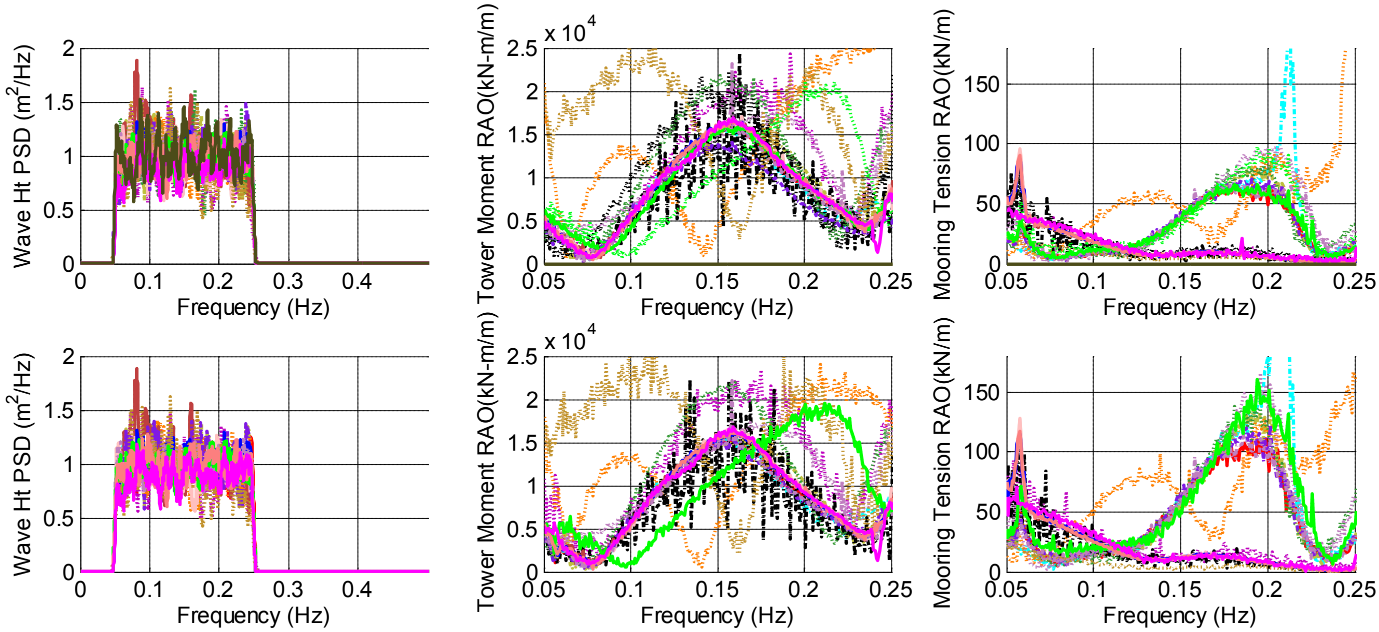

Figure 13: RAO comparisons without wind (top row – load case 2.6) and with wind (bottom row – load case 3.7) for select outputs

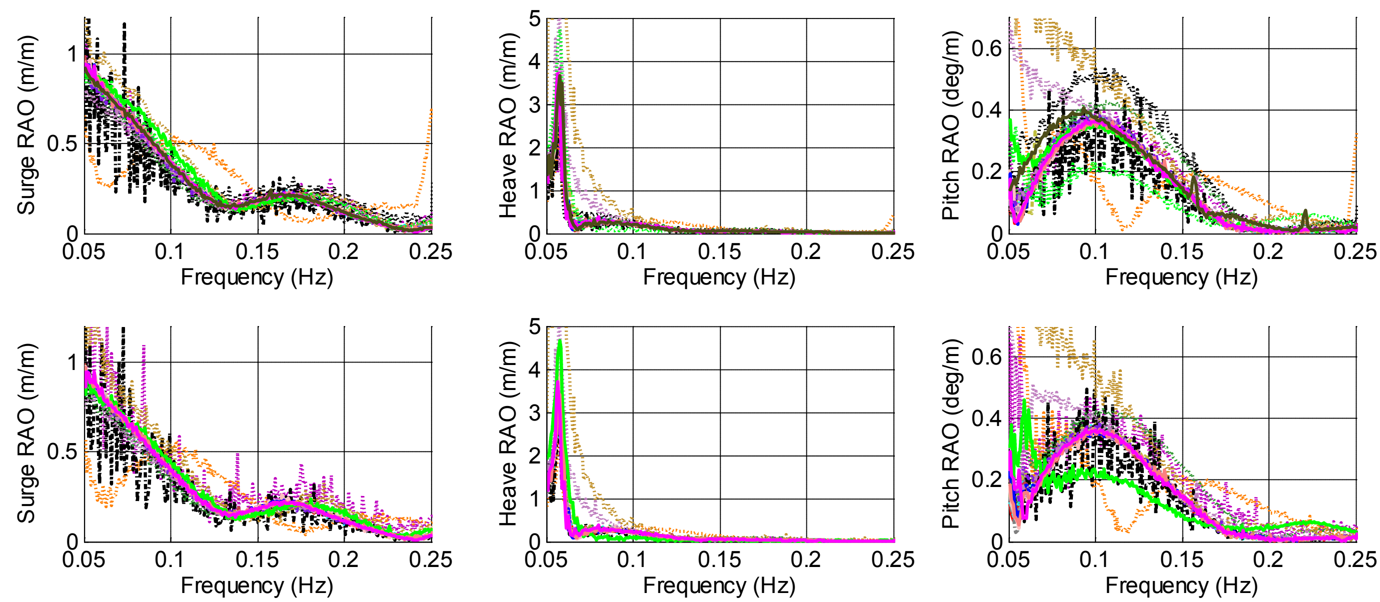

Figure 14: RAO comparisons without wind (top row – load case 2.6) and with wind (bottom row – load case 3.7) for platform motion

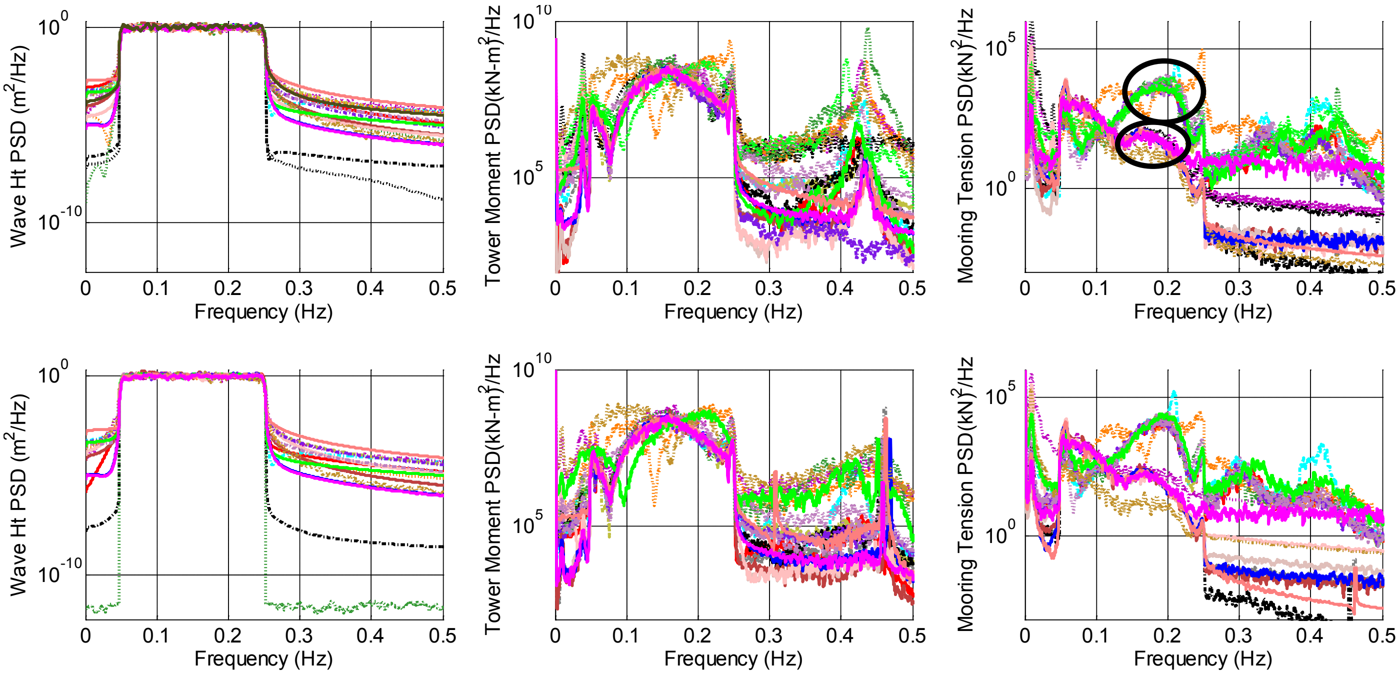

Figure 15: PSD comparisons without wind (top row – load case 2.6) and with wind (bottom row – load case 3.7) for select outputs

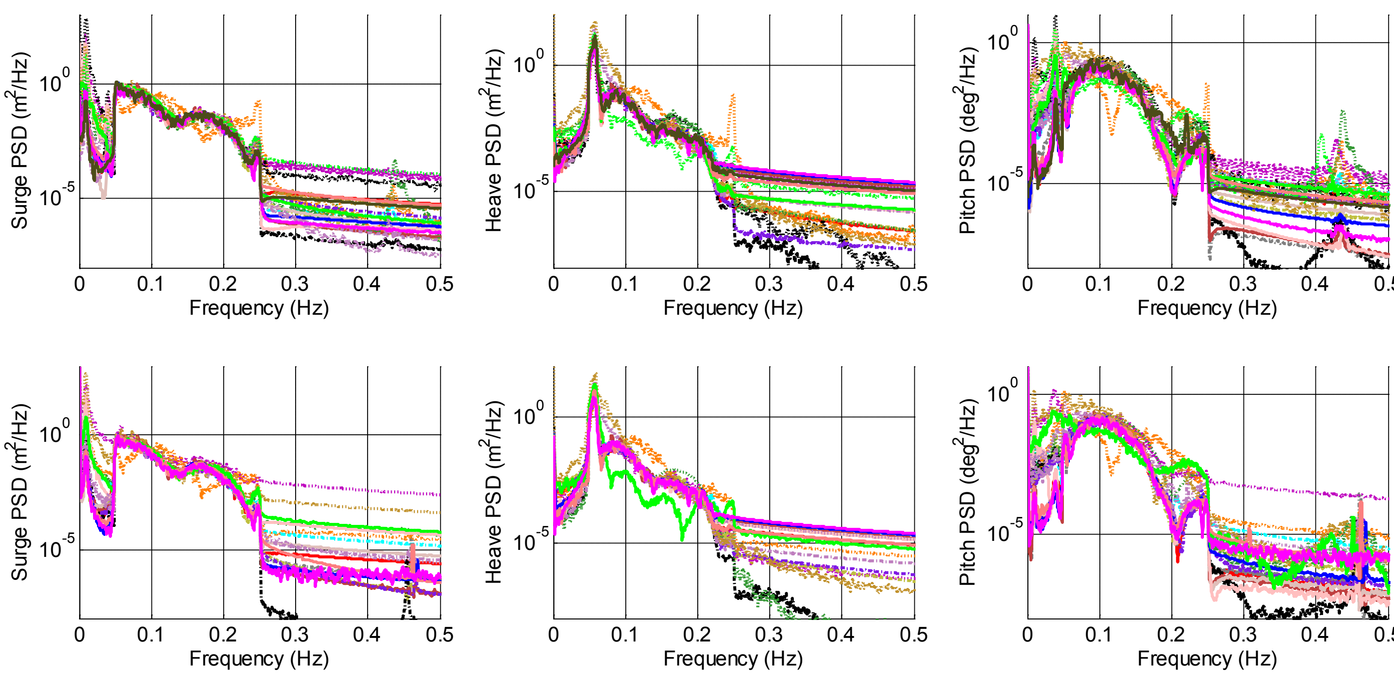

Figure 16: PSD comparisons without wind (top row – load case 2.6) and with wind (bottom row – load case 3.7) for platform motion

Damage Case (Load Case 3.8)

Damage cases were also modeled, which included the loss of a mooring line and the flooding of one column, to check the simulation tools' capabilities in assessing system behavior in a variety of design conditions.

Figure 17 and Figure 18 show some exemplary results from load case 3.8, which entailed the sudden loss of mooring line 1 60 s after the start of the simulation, and included excitation from both steady wind (8 m/s) and regular waves (H = 6 m, T = 10 s). (Mooring line 1 is downwind and to the left when looking downwind.) The roll response of the structure (Figure 17) has an initial transient just after the loss of the mooring, but the large response quickly dies out for most codes. Only for results from the FAST simulation code does the roll response begin to grow again – at around 300 s. This instability appears to be tied to the use of the quadratic drag matrix and disappears when Morison drag is used instead.

Figure 18 shows the path the semisubmersible takes in the water plane after the failure. There is concern that after such an event the system would become twisted and tangled among the remaining lines, but these simulations show the system floating away from the lost mooring line with minimal rotational motion.

The other damage load case (3.9) simulated in this project examined the response of the semisubmersible during a scenario where water has flooded a compartment within one of the offset columns. Additional water was added to the already ballasted column, but the column was not assumed to be entirely flooded because of compartmentalization within that member. The results of this load case (not shown here) did not show significant effects from the flooding, and in hind-sight, the flooding level may have been too low.

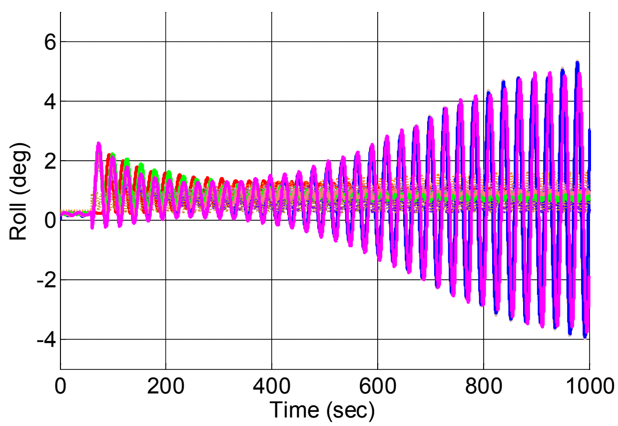

Figure 17: Roll instability in structure after mooring line loss (LC 3.8)

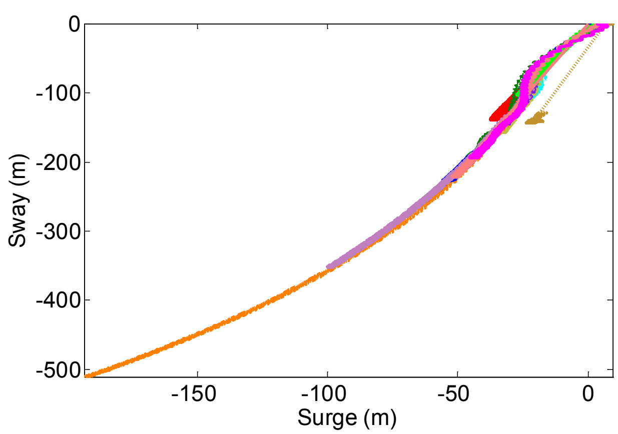

Figure 18: Platform motion in surge/sway plane after mooring line loss (LC 3.8)

CONCLUSIONS

The comparisons performed in Phase II of OC4 and throughout the OC3 and OC4 projects have resulted in a greater understanding of offshore wind turbine dynamics and modeling techniques, and in better knowledge of the validity of various modeling approaches. The results from this project will help guide development and improvement efforts for these tools to ensure that they are providing accurate information to support the design and analysis needs of the offshore wind community.

The following is a list of the main technical findings drawn from Phase II of OC4:

- There is not a clear need for the inclusion of radiation/diffraction loads from a potential-flow theory type solution for this type of semisubmersible under the conditions examined. Morison-only solutions seem to yield similar results, though with more variation in the pitch response. These small differences, however, could be an issue for fatigue, which was not examined in this analysis.
- Approximating the viscous-drag loads for the structure through a global drag matrix may not be sufficient as compared to calculating the member-level Morison drag terms (especially in the presence of large waves and current).
- Varying levels of mean drift resulting from wave excitation are seen among the different models, based on the inclusion of nonlinear hydrodynamics modeling theory. The modeling approaches that create a drift force include wave stretching in Morison's equation, applying loads at the instantaneous position of the structure, including second-order terms in the potential-flow solution, or calculating the mean drift force from the linear potential-flow solution. The drift force is masked by wind loads when the turbine is operating.
- Those codes using a Morison-only approach for modeling the hydrodynamic loads need to be augmented with calculations of the dynamic pressure on the base columns (or heave plates) of the semisubmersible to obtain accurate heave excitation in the system from waves. The need is significant for this structure because of its shallow draft.
- Mooring loads in frequencies above the linear wave range differ significantly between codes using a quasi-static model and those using a dynamic model. These loads have not been seen to have a significant impact on the system dynamics, but they are important in assessing ultimate and fatigue loads in the mooring lines.
- The predicted out-of-plane motion of the blades is slightly smaller for codes using a dynamic wake approach instead of the quasi-steady theory for the aerodynamic induction model, especially in the higher frequency range.
- RAOs are a good way of concisely examining the response characteristics of a floating wind system across a range of wave conditions and comparing the response characteristics between codes (both without and with wind loading).

- The sudden loss of a mooring line for a semisubmersible system does not appear to result in significant loading to the system during the event.
- The partial flooding of one column was not seen to be very significant in the overall response of the system, but the level of flooding examined may have been too low.

The OC3 and OC4 projects have been extremely useful in showing the influence of different modeling approaches on the simulated response of an offshore wind system. Code-to-code comparisons, though, can only identify differences. They do not determine which solution is the most accurate. To address this limitation, IEA Wind has just approved a new project named the Offshore Code Comparison Collaboration Continuation, with Correlation (OC5). This project will begin the validation of offshore wind modeling tools through the comparison of simulated responses to physical response data from actual measurements. It will start in 2014 and run for 4 years. The project will examine three structures using data from both floating and fixed-bottom systems, and from both scaled tank testing and full-scale, open-ocean testing.

ACKNOWLEDGMENTS

This work was supported by the U.S. Department of Energy under Contract No. DE-AC36-08-GO28308 with the National Renewable Energy Laboratory.

REFERENCES

[1] Goupee, A.J., Koo, B.J., Lambrakos, K.F. and Kimball, R.W., 2012, "Model Tests for Three Floating Wind Turbine Concepts," *Proc. 2012 Offshore Technology Conference*, Houston, Texas.

[2] Jonkman, J. and Musial, W., 2010, "IEA Wind Task 23: Offshore Wind Technology and Deployment, Substask 2: The Offshore Code Comparison Collaboration (OC3)," NREL/TP-5000-48191. Golden, CO: National Renewable Energy Laboratory.

[3] Robertson, A.; Jonkman, J; Masciola, M.; Song, H.; Goupee, A.; Coulling, A.; and Luan, C., 2014, "Definition of the Semisubmersible Floating System for Phase II of OC4," *to be published as NREL Technical Report*.

[4] Jonkman, J.M., Butterfield, S., Musial, W. and Scott, G., 2007, "Definition of a 5-MW Reference Wind Turbine for Offshore System Development," NREL/TP-500-38060. Golden, CO: National Renewable Energy Laboratory.

[5] Website for OC4 project: http://oc4.collaborationhost.net. An anonymous login may be used to view results from the project on this site:
login: anonymous@oc4.collaborationhost.net
password: changeit2

[6] Ramachandran, G.; Robertson, A.; and Jonkman, J., 2013, "Investigation of RAOs computed using WAMIT and FAST for various floating offshore wind turbines subjected to different wind and wave conditions," *Proc. 23rd International Offshore and Polar Engineering Conference*, Anchorage, Alaska.